Journal of Applied Polymer Science

Shear flow-induced orientation and structural recovery of multiwalled carbon nanotube in poly(ethylene oxide) matrix

Behnaz Ranjbar, Hossein Nazockdast
Department of Polymer Engineering, Amirkabir University of Technology, Tehran, Iran
Correspondence to: H. Nazockdast (E-mail: nazdast@aut.ac.ir)

ABSTRACT: In the present work we studied the flow induced multiwalled carbon nanotube (MWCNT) orientation and the mechanisms governing the kinetics of nanotube reorientation and three-dimensional network restructuring in poly(ethylene oxide) (PEO)/MWCNT nanocomposites. For this purpose, the linear and nonlinear viscoelastic experiments including frequency sweep, time sweep and transient tests were performed on PEO/MWCNT samples varying in MWCNT content. The extent as well as kinetics of network restructuring was found to be strongly dependent upon the amount of preshearing (shear rate and shearing time) and MWCNT concentration. The results also showed two mechanisms for structural recovery; a fast restructuring at the beginning due to rejoining of clusters and unoriented adjacent nanotube and much slower recovery in the longer annealing times due to Brownian motion. The latter mechanism was found to be uncompleted over 3600 s annealing. This was supported by a_{ij} (orientation tensors) calculated based on transmission electron micrograph. © 2015 Wiley Periodicals, Inc. J. Appl. Polym. Sci. **2015**, *132*, 41753.

KEYWORDS: kinetics; rheology; structure; property relations

Received 10 August 2014; accepted 12 November 2014
DOI: 10.1002/app.41753

INTRODUCTION

Nanoparticle containing polymers offer a great potential of polymer composites with remarkably enhanced properties. The excellent physical and mechanical properties exhibited by multiwalled carbon nanotube (MWCNT) make them to be one of the most useful building blocks candidates for producing new generation of materials for a variety of applications.[1,2] The great interest in using carbon nanotubes in polymeric matrices is due to their outstanding potential to produce polymer-nanocomposites with enhanced electrical, thermal and mechanical properties at low nanoparticle concentrations.[2]

The degree of success in reaching the desirable enhancement in these nanocomposites is highly dependent on state of MWCNT dispersion which itself is controlled by MWCNT aspect ratio, orientation, concentration, and processing history. These factors also affect the inter-particle interactions and the probability of the formation of an interconnected network of particles in the matrix. It has been well recognized that there is a MWCNT concentration above which a three-dimensional (3D) network can be formed through particle–particle and/or particle–matrix interconnectivity.[3] This concentration is known as rheological percolation threshold. The properties of MWCNT suspensions in the matrices with different polarities have been studied by many researchers.[4–12]

The rheology has proved to be one of the strongest tools to be used for studying the nanoscopic structure of polymer nanocomposites.[4–6,11] Small amplitude oscillatory shear measurements (linear viscoelastic analysis) are commonly used due to its great sensitivity to microstructure including the state of nanoparticle dispersion and the extent of orientation; while the transient measurements (nonlinear viscoelastic analysis) can provide more insight into understanding the nanoscopic structure through microstructural changes at larger deformations.

The flow induces anisometric nanoparticles such as multi walled carbon nanotubes (MWCNT) can play a significant role in determining electrical,[4] thermal conductivity,[13] and mechanical performance[8] of the nanocomposite. Thostenson and Chou[8] found that, in MWCNT/poly(styrene) nanocomposites, when MWCNTs are oriented in one direction, the storage modulus is improved by 49% compared to the 10% improvement in randomly oriented nanotubes. Wang *et al.*[13] found much higher thermal conductivity in aligned MWCNTs over random ones. It has been shown that the rheological technique can also provide reliable information about the flow induced orientation and restructuring of asymmetric particle containing nanocomposites.[4–6,14,15]

The melt rheological percolation threshold of nanoparticle containing polymers is the concentration above which nanocomposite behavior changes from liquid-like to pseudosolid-like due

to the 3D network formation originate by particle–particle and/or particle–polymer chain interconnectivity. Percolation is well understood in sphere and ellipsoids fillers.[16] The percolation threshold is determined by the aspect ratio and the state of dispersion of nanoparticles which is highly dependent on the affinity of nanoparticles and polymer matrix. The particle alignment also influences the percolation threshold. The higher the orientation of the particles, the larger will be the percolation threshold.[14,17] In order to obtain full control on nanocomposite properties, the nanotube orientation should be controlled tightly.

In nanoclay–polymer nanocomposites, rheological characteristics are often related to the interlayer distance and the nanoparticle network structure. Transient rheological phenomena can be explained based on exact description of these two factors.[15]

For colloidal suspensions, Brownian forces are counterbalanced under flow by hydrodynamic forces. The relative balance between these two is expressed by the Peclet number ($\mathrm{Pe}=\dot{\gamma}/D_r$), where $\dot{\gamma}$ is the shear rate and D_r is the rotary diffusion coefficient. The D_r of the particles can be calculated as $D_r=3k_BT/4\eta a^3$,[18] where k_B is the Boltzmann constant, T is the absolute temperature, η is the viscosity of the matrix, and a is the aspect ratio. In the case of suspensions containing ellipsoidal particles, with aspect ratio "r" the rotary diffusion is given by Perrin equation [eq. (1)].[19]

$$D_r=\frac{k_BT}{8\pi\eta a^3}\left\{\frac{3}{2}\frac{((2-(1/r^2))/(\sqrt{1-(1/r^2)}))\ln\left[r(1+\sqrt{1-(1/r^2)})\right]-1}{1-(1/r^4)}\right\} \quad (1)$$

Ren and Krishnamoorti[18] used linear viscoelastic measurements to study the kinetics of structural relaxation in clay nanocomposites. They found that the dimensions of the silicate layers, viscoelasticity, temperature, and molecular weight of the polymer matrix do not influence the increase in the storage modulus during annealing after preshear considerably. They concluded that, Brownian randomization is not the major mechanism of structural changes in these systems.

Solomon *et al.*[20] observed that the rest time before reversal directly affects the stress overshoots following reversal of steady shear flow. The magnitude of the overshoot increased as the rest time increased, but, over time, the scales were much shorter than that expected for Brownian rotation in such systems. They concluded that the reorientation of structure was affected by attractive interactions between the clay platelets and not Brownian motion.

Lele *et al.*[21] reported the relaxation of orientation after steady preshearing as measured by rheology and *in situ* X-ray diffraction (XRD). They confirmed the conclusion of Ren and Krishnamoorti[18] that relaxation time-scale measurement using rheo-XRD was much faster than the expected Brownian relaxation time ($1/D_r$). They concluded that the rapid relaxation of nanoparticle orientation is resulted by the relaxation of the stress in polymeric chains of the matrix. They also concluded that the attractive interactions do not play an important role in relaxation of nanoparticle orientation because the uncompatibilized dispersions showed slower relaxation than the compatibilized one.

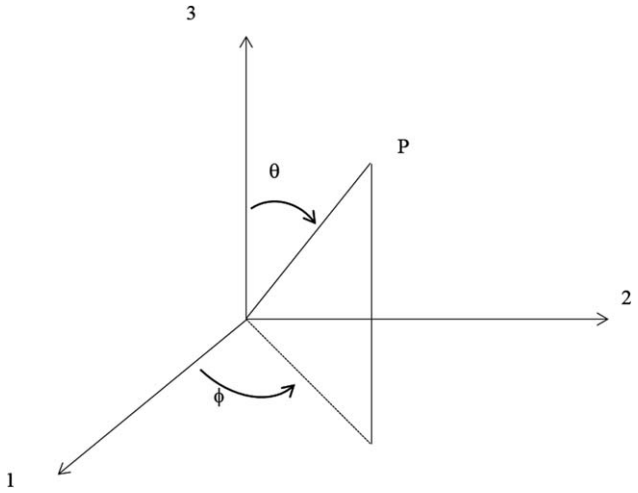

Figure 1. Orientation vector in Cartesian coordinate frame.

In a theoretical approach, it has been shown that[3] the orientation of a single fiber can be described by unit vector u along the fiber axis, as shown in Figure 1. The components of unit vector P in the coordinate directions are

$$P_1=\sin\theta\cos\phi \quad (2)$$

$$P_2=\sin\theta\sin\phi \quad (3)$$

$$P_3=\cos\theta \quad (4)$$

Accordingly, the average orientation of a large number of fibers of similar length can be described using distribution function, $\Psi(\theta,\phi)$. A compact way to represent the average orientation state is using second- and fourth-order orientation tensors, which are defined as the second and fourth moments of the orientation distribution function.[3] Another condition arising from the physical reality is that all fibers have a direction that the integral of the distribution function over all directions can be normalized to unity.

$$\int_0^{2\pi}\int_0^{\pi}\psi(\theta,\phi)\sin\theta d\ \theta d\phi=1.0 \quad (5)$$

Fiber orientation can be described completely and unambiguously using a distribution function. Unfortunately the prediction and interpretation of the distribution function is not convenient. A number of orientation parameters have been suggested to easily interpret measures of orientation. Recently, the second moments of the distribution function and second-order orientation tensors have been used to represent orientation. A compact, efficient, and convenient representation of the distribution function can be done using orientation tensors. The components of this second-order tensor, a_{ij}, are

$$\langle a_{ij}\rangle=\int_0^{2\pi}\int_0^{\pi}g\psi(\theta,\phi)\sin\theta d\ \theta d\phi \quad (6)$$

where $<a_{ij}>$ is the average of g over all directions, weighted by the probability distribution function.

Nazockdast and Nazockdast[22] calculated orientation tensors a_{ij} and a_{ijkl} as a function of time. They adopted the Folgar–Tucker[23] equation and IBOF closure approximation to calculate these components and the Lipscomb *et al.*[24] constitutive

equation to calculate hydrodynamic stress. The modeling results suggested that the dynamics of polymer chains slows as the result of polymer/organoclay interaction and a network-like structure is formed polymer/clay interaction rather than interparticle interaction.

It has been shown that the reorientation of anisometric nanoparticles stems from the relaxation of the polymer matrix[15,21] and the reconstruction of the network.[25] The mechanism is dependent upon the particle type and the rheological behavior of polymer matrix. Moreover, in contrary to fiber suspensions, Brownian motion and particle/particle attractive forces play the important role in reorientation and structural build-up in MWCNT containing nanocomposites.[26]

Poly(ethylene oxide) (PEO), which is used in the present study, is a polar, semicrystalline polymer which is water soluble and nonionic. It can be used as a flocculent, thickening agent, sustained-release matrix, lubricating agent, dispersing agent, and water-retention compound. Its hydrophilicity, biocompatibility, and versatility make it attractive as a biomaterial mainly used in sustained-release matrix systems, transdermal drug delivery systems,[27] and mucosal bioadhesives. PEO is a favorable candidate for the development of solid polymer electrolytes with high ionic conductivity because of its ability to dissolve large amounts of salt and its structure, which supports ion transport.[28] There are a limited number of studies focusing on rheological characterization of dispersion of carbon nanotubes in PEO with melt compounding method.[29]

In the present study we used transient shear viscosity to characterize the orientation behavior of PEO/MWCNT nanocomposites. The kinetics of reorientation and reformation of the MWCNT particles in a polymer melt were examined using time-resolved measurements of the dynamic shear modulus after well-defined shear deformation at above and below the percolation threshold.

EXPERIMENTAL

PEO with an average molecular weight of 10,0000 g mol^{-1} and melting temperature of 65°C was purchased from Aldrich and used as received. . Multi-walled carbon nanotubes (MWCNTs) with the trade name Nanocyl NC 7000 were used as the dispersed phase. PEO/MWCNT nanocomposite samples with MWCNT concentrations from 0 to 2 were considered. All samples were prepared using the melt-compounding method using a laboratory internal mixer (Braebender Plasticorder W50). Melt-compounding was carried out in a 60 cm^3 internal mixer equipped with a Banbury-type rotor design at 110°C and rotor speed of 100 rpm for 12 min.

All of the rheological measurements were performed on samples using a rotational and oscillatory rheometer (PaarPhysica UDS 200). All the measurements were conducted under N_2 atmosphere using a cone and plate geometry with a diameter of 50 mm and a cone angle of 2°. The measurements were performed at 110, 140, and 180°C. Disk-like samples 50 mm in diameter and 0.5 mm in thickness were prepared by compression molding of the granulated samples prepared in an internal mixer. A time sweep experiment was performed on all the samples at 110, 140, and 180°C under nitrogen purge confirming the absence of any degradation during the course of the measurements. To ensure to be in linear viscoelastic region, an amplitude sweep experiment was performed at 140°C on the sample with 2 wt % MWCNT. Results of amplitude sweep tests showed that amplitude of 0.5% is small enough to keep the deformation in the linear viscoelastic region and produce reliable signals during measurement. The linear viscoelastic properties of the samples were studied using small amplitude oscillatory shear experiment. The measurements were performed in a fixed strain ($\gamma = 0.5$) and frequency range of 0.1–10,000.

The structural evolution of the nanocomposites was monitored utilizing transient rheological experiment. In this test, samples were initially presheared at different shear rates in the clockwise direction for 300, 500 and 1000 s. This was followed by different rest times (1, 1000 and 3600 s) after cessation of flow and monitoring of stress relaxation.

The stress growth measurement after preshearing was performed in the counter clockwise direction at the same shear rate up to steady state conditions. Rest times varying from 1 to 3600 s were applied and the sample response was monitored by transient measurement in the reverse direction.

In another set of experiment, samples were presheared at different shear rates and a time sweep experiment was performed immediately after preshearing, in order to quantify the extent of reorientation. The storage modulus was measured against time in an angular frequency of 0.5 s^{-1}; the independency of the storage modulus against time guaranteed microstructural stability after annealing.

For transmission electron microscopy (TEM), the presheared samples were prepared by shearing the samples at 1 s^{-1} for 300 s at 140°C. The shearing action was stopped and the sample was blown by nitrogen gas to quickly cool to room temperature. The cooled sample was then microtomed using a diamond knife parallel to the flow direction. The nanostructure and local orientation of the MWCNT were examined using TEM (Philips, em2085) with an accelerator voltage of 100 kV. The orientation angle of the MWCNTs was measured by Screen Protractor v1.1 software.

RESULTS AND DISCUSSION

Melt linear viscoelastic measurements were conducted in conjunction with nonlinear rheological experiments in order to study the effect of flow history on MWCNTs orientation and reorientation.

In order to determine the linear viscoelastic region, an amplitude sweep experiment was applied on the samples. The linear viscoelastic region for the samples was determined through the plot of G' versus strain as shown in Figure 2. As this region is shortened by MWCNT concentration[30] we chosed the sample with the highest MWCNT content (2 wt %). Therefore, all the linear viscoelastic measurements were performed blow the critical strain of this sample (0.5%).

Figure 3 shows the storage modulus (G') as a function of frequency for the virgin PEO and the nanocomposites containing

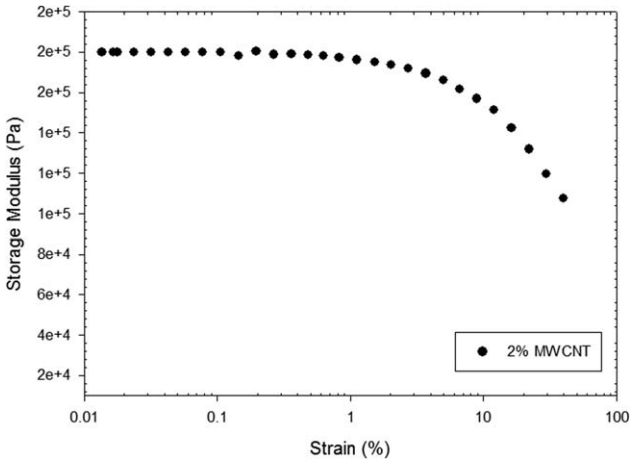

Figure 2. Amplitude sweep measurement on the nanocomposite sample containing 2 wt % MWCNT at 140°C and angular frequency of 1 rad s^{-1}.

0.5, 1, 1.5 and 2 wt % of MWCNT at 140°C. As it can be seen, while the 0.5% MWCNT containing sample exhibits a rheological behavior similar to that of the PEO matrix, the samples with higher MWCNT concentration show a pronounced low frequency nonterminal storage modulus whose extent increases with increasing with MWCNT concentration. The solid-like behavior observed at low frequencies is an indication of a percolation threshold. Such a low rheological percolation threshold found for these samples has also been reported for other MWCNT containing polar polymer matrices.[29] It has been attributed to great affinity of MWCNT with polar PEO matrix.

Figure 4 shows the plot of storage modulus (obtained from Figure 3) versus normalized MWCNT concentration measured at the frequency of 0.14 s^{-1} for PEO/MWCNT samples. It is generally known that in the vicinity of percolation threshold one can use a scaling low in the case of randomly distributed anisometric particles. Many researchers have used the plot of G' versus nanoparticle concentration to evaluate the rheological percolation threshold.[31,32] This can be expressed as

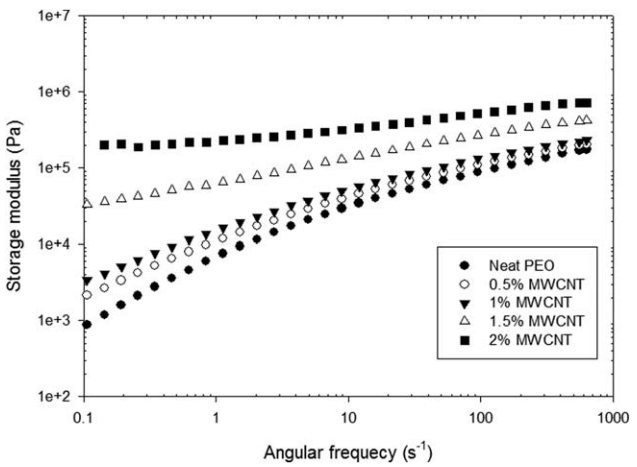

Figure 3. Plot of storage modulus versus angular frequency for the nanocomposite samples containing different MWCNT loading.

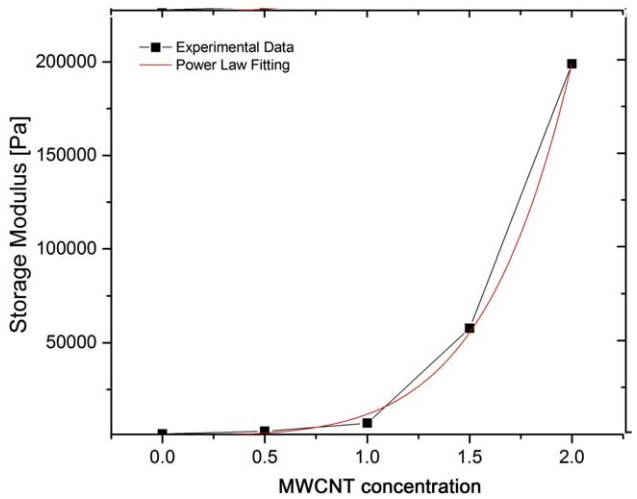

Figure 4. Fitting the power law model to the experimental data to obtain the percolation threshold. [Color figure can be viewed in the online issue, which is available at wileyonlinelibrary.com.]

$$G' \sim (\phi - \phi_c)^t \quad (7)$$

where G' is the storage modulus of the nanocomposite, ϕ is the MWCNT weight fraction, and ϕ_c is the percolation critical concentration. By using a curve fitting software (Origin 9.1) 1.14 was reported as ϕ_c the percolation threshold.

The structural evolution of the nanocomposites was monitored using transient rheological testing. The results of stress overshoot experiment performed on the nanocomposite samples in the form of shear stress as a function of shearing time are shown in Figure 5. These figure show that the samples presheared with 0.3 s^{-1} does not show a pronounced stress overshoot compared to other samples. This indicated that for these nanocomposite samples there is a minimum limit of shear rate below which no orientation could occur. These results are in agreement with those reported by Khalkhal and Carreau[26] for epoxy/MWCNT sample. The minimum shear rate may depend on the MWCNT aspect ratio as well as matrix–nanoparticle interaction. In other words, with increasing the network

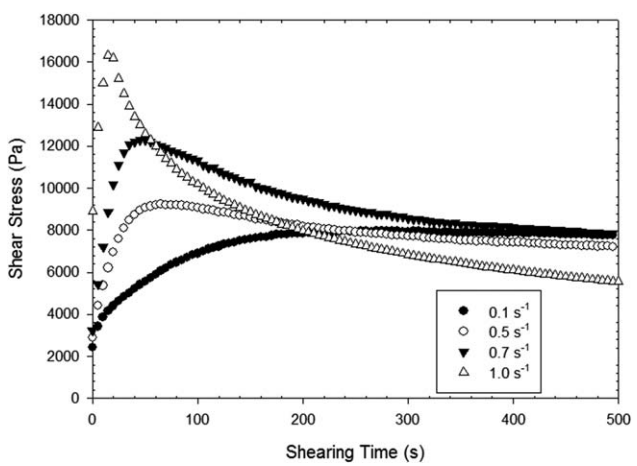

Figure 5. Stress as a function of time for 1.5 wt % nanocomposite at $T = 140$°C at different shear rates.

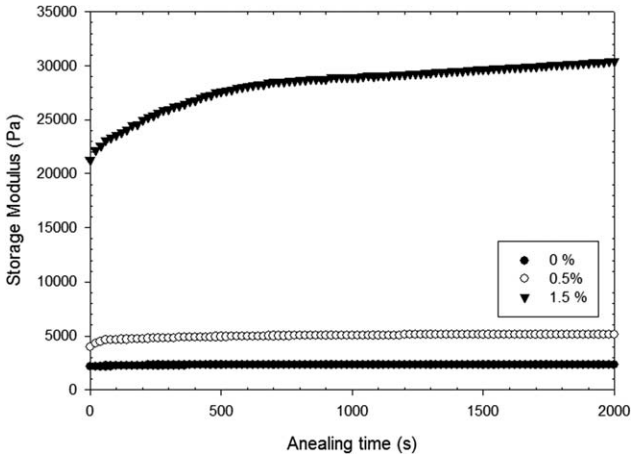

Figure 6. Storage modulus recovery after cessation of flow with shear rate = 1 s^{-1} for 300 s for different concentration of MWCNT.

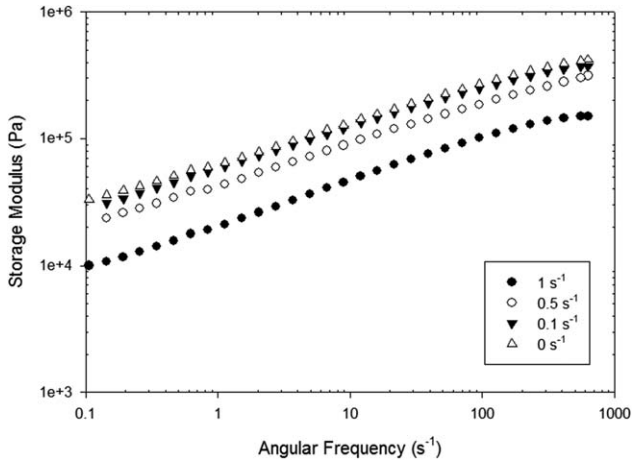

Figure 7. Storage modulus versus angular frequency for PEO containing 1.5 wt % MWCNT before and immediately after steady shear deformation.

strength, the shear rate required for destroying the network increases.

As mentioned earlier the final nanoorientation remained in the nanocomposite samples is determined by the extent of initial flow induced orientation and nanotube reorientation after cessation of flow in isothermal process and cooling rate in nonisothermal condition.

In order to provide more insight into understanding the real mechanism of MWCNT reorientation and restructuring, a set of time sweep experiments were performed on the samples after cessation of flow. Figure 6 shows the recovery of storage modulus versus annealing time for the neat PEO and its nanocomposite samples below and above their percolation threshold at steady shear of 1 s^{-1} and $T = 140°C$. From these results one can notice that while the neat PEO and the sample below the percolation concentration show smooth increase in modulus, the samples above their percolation threshold exhibit a fast initial recovery in storage modulus followed with smooth increase at longer annealing time. While the PEO matrix did not exhibit a stress overshoot at this shear rate, an overshoot was systematically observed for each initial stress growth experiment for the PEO/MWCNT nanocomposites. From these results we can suggest that for PEO samples molecular relaxation has negligible contribution in the storage modulus recovery value. The results of sample containing 0.5% MWCNT (below percolation threshold) reveal that nanotube orientation does not have appreciable contribution on the storage modulus recovery. Therefore, we can conclude that fast recovery of storage modulus occurred at short initial times, for the sample above the percolation threshold is mainly attributed to the network restructuring.

Figure 7 shows storage modulus versus frequency measured immediately before and after steady shear at 0.1, 0.5, and 1 s^{-1}. As can be seen, increasing the shear rates, leads to greater extent of 3D network breaking down and/or nanotube orientation both resulting in decrease in the storage modulus. The results of Storage modulus recovery as a function of annealing time at various shear rates at 140°C are shown in Figure 8. As it can be seen the trend of the sample presheared at shear rate of 0.1 s^{-1} is different from those presheared at higher shear rates. On the other hand, the 3D network structure of the 1.5% MWCNT containing sample remains almost intact at this extent of shear rate. This supports our above-mentioned discussion stating that MWCNT reorientation and structural recovery after cessation of flow is controlled by two mechanisms (fast and slow recovery) depending on the time scale.

In order to study the effect of rest time on reorientation kinetics, the samples were sheared for a constant shearing time (300 s) at 1 s^{-1} then it was allowed to rest for a certain time (1–3600 s). Next, the response was monitored by transient measurement in the reverse direction. It should be noted that for each experiment a new sample was used.

As it can be seen in Figure 9 the values of overshoots were highly dependent on rest time; the transient stress overshoot is not visible for short rest times, but increased regularly as rest time increased. However, the overshoot peak did not reach the value that observed during the first start-up even at the longest

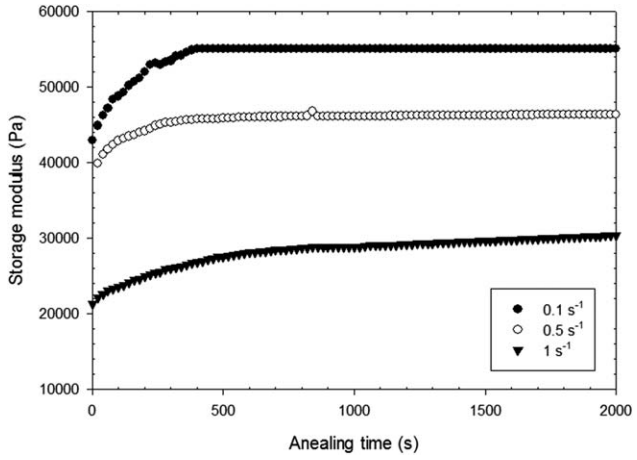

Figure 8. Storage modulus recovery of PEO containing 1.5 wt % MWCNT as a function of annealing time after different shear rates for 300 s at $T = 140°C$.

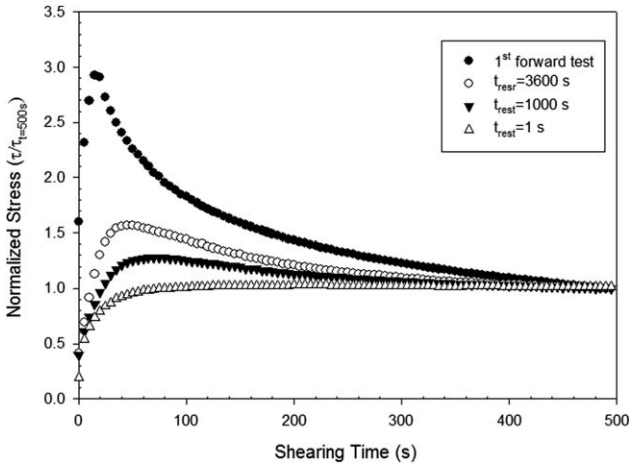

Figure 9. Normalized shear stress as a function of shearing time for reverse start-up following initial forward experiment at $T = 140°C$ and shear rate of 1 s^{-1} after different rest times.

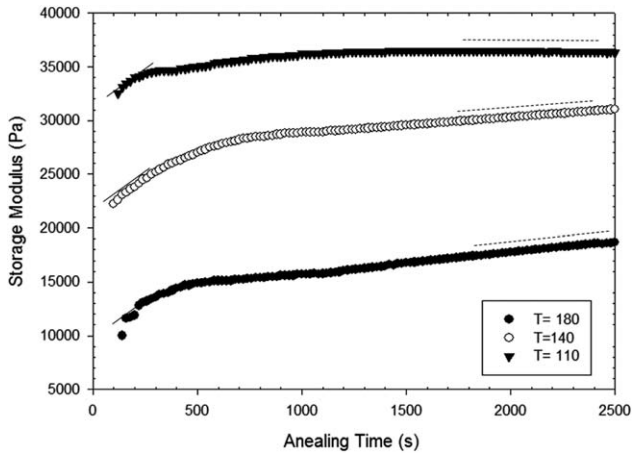

Figure 10. Storage modulus recovery of PEO containing 1.5 wt % MWCNT as a function of temperature after shear rate of 1 s^{-1} for 300 s.

rest time (3600 s). This is in agreement with the results reported by Pujari *et al.* for epoxy/MWCNT[33] and poly(butene)/clay[34] systems but disagrees with the results reported by Letwimolnun[15] on PP/PP-g-MA/cloisite 20A nanocomposite whose samples became fully isotropic after being presheared and the network restored after 1200 s. After a short rest time, the MWCNT particles maintained their orientation and hence no overshoot could be observed. As the rest time increased, the MWCNTs lost their orientation, partially returned to random distribution, and rebuilt the network structure.

According to Cassagnau[35] nanostructure recovery is mainly due to particle–particle attractive forces.

On the other hand, Eslami *et al.*[36] and Kalfus and Jancar[37] show that the matrix chain relaxation can also play a part in reorientation and structural recovery. In other words, temperature can affect the viscosity of matrix and therefore chain relaxation. It is worth mentioning that, temperature dependency of viscosity (activation energy) of nanocomposites can be considered as a measure of nanoparticle/matrix interaction, which itself can influence the nanocomposite reorientation.

Figure 10 shows the storage modulus recovery versus annealing time for the samples containing the same nanotube loading (1.5%) and 300 s preshearing at shear rate of 1 s^{-1} at three different temperatures. It appears that fast storage modulus recovery (occurred at short times) is almost independent of temperature while the slower storage modulus growth taking place at longer annealing times (the dashed line in Figure 10), slightly increases with increasing the temperature (the solid line in Figure 10).

The temperature dependency of polymers is determined through well-known Arrhenius equation as

$$\eta_{app}(T) = Ke^{E_a/RT} \quad (8)$$

where η_{app} is the apparent shear viscosity at a specific shear rate; R is the molar gas constant (8.314 J mol^{-1} K^{-1}); and T is temperature (K). K can be obtained from the slope of $\ln(\eta_{app})$ versus $1/T$ which is calculated from the slope obtained using the linear regression of the plot of log η_{app} versus $1/T$ are summarized in Table I. As one can find from the table, the activation energy of the PEO/MWCNT composites increased as the MWCNT loading increased, suggesting that the incorporation of MWCNT into the PEO matrix slows down the dynamic of matrix and this effect is intensified with increasing MWCNT loading. The activation energy of the neat PEO is 7.88 kJ mol^{-1} which is increased to 10.2 kJ mol^{-1} by incorporating 0.5% of MWCNT and to 20.4 kJ mol^{-1} by incorporating 1% MWCNT. The activation energy of PEO accounts for about 75% of the total activation energy of the 0.5% nanocomposite and for about 39% of the total activation energy of the 1% MWCNT nanocomposite.

The addition of nanotubes caused a large energy barrier to segmental motion of the polymer chain in a confined space and increased the flow activation energy. The data given in Table I also show that the activation energy of the nanocomposite samples decrease after being presheared. This can be attributed to the structural breakdown resulting in higher extent of chain mobility in the system. However, the resulting decrease in activation energy induced by structural breakdown did not reach to that of unsheared samples; the results support the results shown in Figures 9 and 10 discussed previously.

Table I. The Activation Energy E_a for MWCNT/PEO Composites with Different MWCNT Loadings at 140°C

Samples	Test condition	E_a (kJ mol^{-1})
Neat PEO	Before steady shear	7.88
PEO-MWCNT 0.5 wt %	Before steady shear	10.2
PEO-MWCNT 0.5 wt %	After steady shear[a]	8.1
PEO-MWCNT 0.5 wt %	Recovered[b]	8.7
PEO-MWCNT 1.5 wt %	Before steady shear	20.4
PEO-MWCNT 1.5 wt %	After steady shear	14.9
PEO-MWCNT 1.5 wt %	Recovered	16.8

[a] At the shear rate of 1 s^{-1} for 300 s.
[b] At the shear rate of 1 s^{-1} for 300 s then 3600 s annealing.

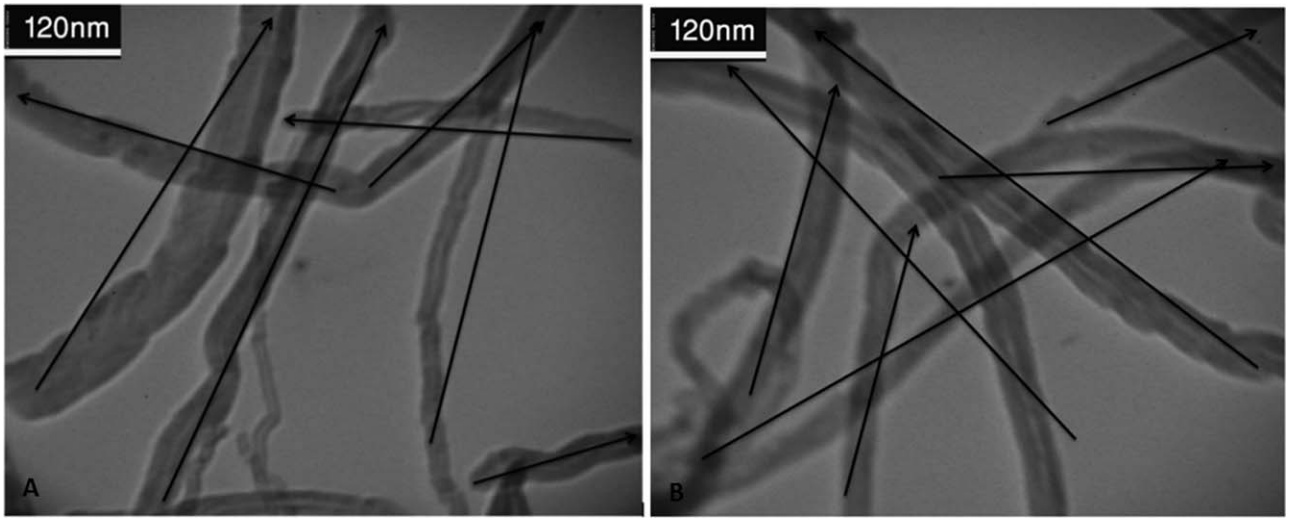

Figure 11. Characterization of MWCNT orientation state with TEM image. (a) Sheared sample. (b) Recovered sample at 140°C, shear rate of 1 s^{-1} and 1.5 wt % MWCNT.

In the present study an attempt was also made to evaluate the MWCNT orientation state in 2D plane by using Tacker and Advani's approach[3] described in introduction section. For this purpose, eqs. (2)–(4) are reduced to

$$P_1 = \sin\theta, P_2 = \cos\theta \tag{9}$$

This description was adapted from fibers to characterize 2D MWCNT orientation. To measure the components of orientation experimentally, the orientation angle of each individual nanotube was measured in the TEM image. If the number of MWCNT particles in a TEM image is N, then a_{ij} (orientation tensor) in that region can be calculated as[3,23]

$$a_{ij} = \frac{1}{N}\sum_{k=1}^{N} p_i^k p_j^k \tag{10}$$

This equation represents orientation state a_{ij} of the sample containing N nanotubes. In case of a 2D orientation field, there are only two independent components, such that $a_{21} = a_{12}$ and $a_{11} + a_{22} = 1$. The magnitude and direction of the orientation with respect to coordinate axis 1 is represented by the scalar components of the second-order orientation tensor. a_{ii} and a_{ij} are the magnitude of alignment in the coordinate direction and the deviation of the coordinate axes from the principal axes of orientation, respectively. The components of the orientation tensor in two dimensions are used for drawing an ellipse which graphically describes the orientation.[38]

A typical transmission electron micrograph of sheared and recovered samples containing 1.5% MWCNT is shown in Figure 11. The vectors represent the average direction of nanotubes. The a_{ij} components and a deflection tensor can be calculated from the vectors. For a circle with a radius of unity and the center of intercept, this deflection tensor forms an ellipse in which the major axis represents the preferred orientation of the nanotubes. Numerical values of the minor and major axes of this ellipse are measures of the degree of orientation in that individual direction.[39] The local orientation angle of the MWCNTs was measured using Screen Protractor v1.1 software and eq. (9).

As it can be observed in Figure 11, most MWCNTs show a more or less curved feature. If the curvature of one MWCNT is small, an approximate orientation vector P can be considered which represents the major direction vector of one curved MWCNT. For large curvatures, it is divided into more than one direction vector. The preferred orientation direction and the magnitude of this alignment can be extracted from the ellipse. In Figure 11(a,b), the local orientation tensor is

$$\langle a \rangle = \begin{bmatrix} 0.47 & 0.20 \\ 0.20 & 0.53 \end{bmatrix} \tag{11}$$

for the sheared sample, and

$$\langle a \rangle = \begin{bmatrix} 0.48 & 0.05 \\ 0.05 & 0.52 \end{bmatrix} \tag{12}$$

for the recovered sample. These tensors can be used to draw the ellipse described earlier (Figure 12). It can be concluded that the orientation of MWCNTs was not random after 3600 s recovery. This result is in a good agreement with that from the rheological data in Figure 8.

From what discussed previously, we came to conclusion that when a PEO/MWCNT nanocomposite above its percolation threshold is imposed to steady shear field, the existing 3D network is destroyed resulting in a new structural state consisting of noncontacting clusters, unorientated individual MWCNT and flow induced oriented MWCNTs. It should be noted that the amount of each of these three microstructures is greatly dependent upon the extent of shearing. The kinetic of structural recovery nanotube reorientation and network formation of the PEO/MWCNT nanocomposite samples is governed by two different mechanisms as schematically described in Figure 13: first, a fast 3D network reformation occurs in earlier resting time which is driven by joining the existing clusters and

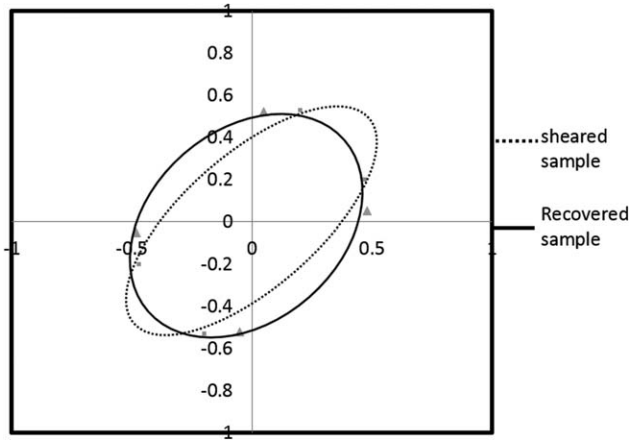

Figure 12. Orientation ellipses of sheared and recovered samples.

aggregation of unoriented adjacent MWCNTs through direct contacting. The contribution of this part of restructuring into total 3D network reformation is strongly dependent upon the extent of preshearing (shear rate and shearing time) and of course the MWCNT concentration. This mechanism of restructuring is mostly caused by particle–particle and/or particle–matrix interaction and Brownian diffusion does not have an appreciable contribution. Second, a much slower structural recovery takes place in longer time through MWCNT reorientation, followed by clustering and finally 3D network formation. This part of restructuring is mostly controlled by Brownian diffusion mechanism.

CONCLUSIONS

The present study examined the multi-walled carbon nanotube (MWCNT) orientation and restructuring in PEO matrix by means of oscillatory and transient viscoelastic analysis along with TEM. The pronounced low-frequency solid body response observed in the linear oscillatory shear test indicated high melt intercalation and good dispersion of nanotubes in the nanocomposite samples which may be a result of high thermodynamic affinity between MWCNT and the PEO matrix. The results of start-up flow tests showed a nonlinear relationship between shear rate and the stress overshoot as a measure of 3D MWCNT network breakdown and/or the particle orientation. From the results of the same experiment, it was found that there is a shear rate below which no appreciable flow-induced orientation could be detected.

The kinetics of storage modulus (G') recovery after flow cessation, was found to be accelerated with increasing temperature. Although the extent of reorientation and restructuring measured as a function of rest time after preshearing was increased with increasing rest time, it did not return to its initial value even after 3600 s. This was evidenced by transmission electron micrographs. The results also showed two distinct rates of structural recovery; a fast restructuring at the beginning and much slower recovery in the longer annealing times. The first recovery was suggested to be due to the rejoining of clusters and unoriented adjacent nanotube, and the slow recovery occurring at longer times was attributed to MWCNT reorientation and 3D network formation both governed by Brownian diffusion mechanism.

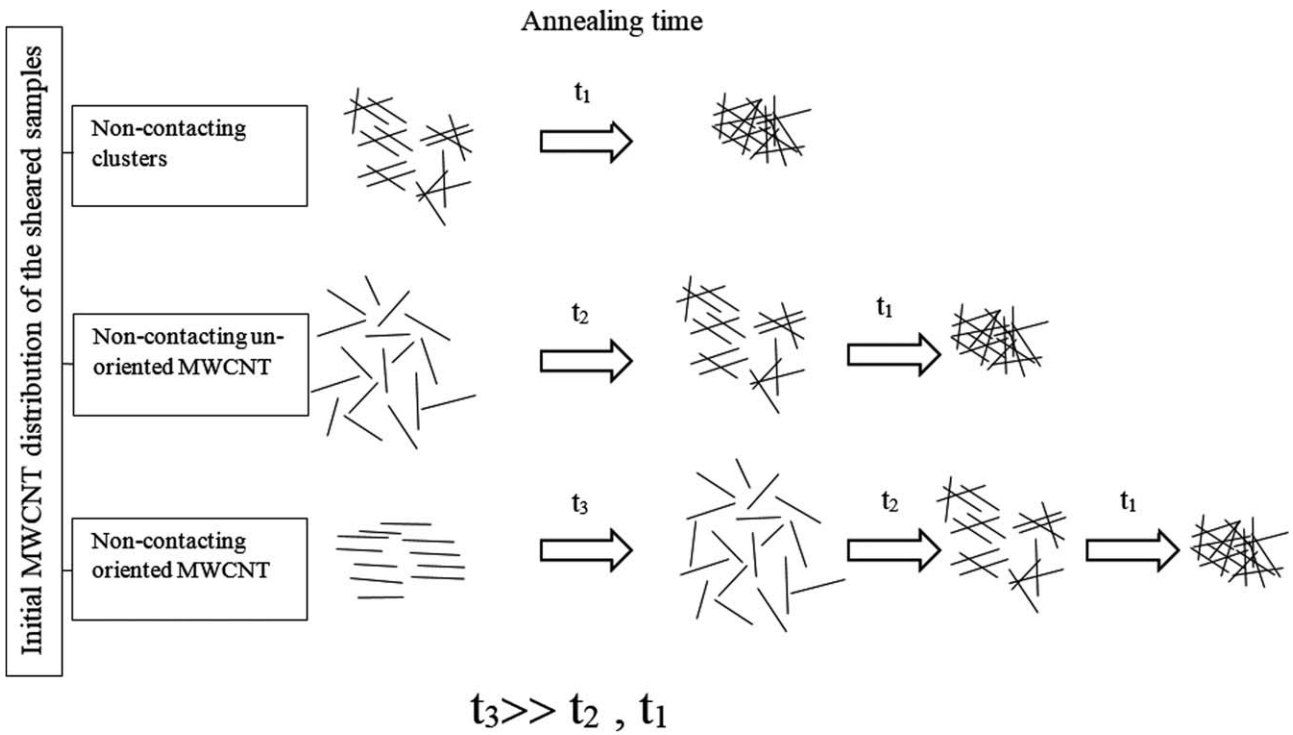

Figure 13. Schematic presentation of the suggested mechanism governing structural recovery of anisotropic particle containing nanocomposites.

REFERENCES

1. Sun, Y.-P.; Fu, K.; Lin, Y.; Huang, W. *Acc. Chem. Res.* **2002**, *35*, 1096.
2. Baughman, R. H.; Zakhidov, A. A.; de Heer, W. A. *Science* **2002**, *297*, 787.
3. Advani, S. G.; Tucker, C. L. *J. Rheol.* **1987**, *31*, 751.
4. Hu, G.; Zhao, C.; Zhang, S.; Yang, M.; Wang, Z. *Polymer* **2006**, *27*, 480.
5. Fan, Z.; Advani, S. G. *J. Rheol.* **2007**, *51*, 585.
6. Tiwari, M. K.; Bazilevsky, A. V.; Yarin, A. L.; Megaridis, C. M. *Rheol. Acta* **2009**, *48*, 597.
7. Hobbie, E. K.; Fry, D. *J. Phys. Rev. Lett.* **2006**, *97*, 036101.
8. Thostenson, E. T.; Chou, T.-W. *J. Phys. D* **2002**,*35*, L77.
9. Sarfraz, H. A.; Ibnelwaleed, A. H.; Anwar, P. *Appl. Polym. Sci.* **2011**, *119*, 290.
10. Sarfraz, H. A.; Abdulhadi, A. A.; Anwar, U. H.; Ibnelwaleed, A. H. *e-Polymers* **2011**, *11*, 722.
11. Sarfraz, H. A.; Ayuba, A. A; Muataz, A.; Anwar, U. H.; Ibnelwaleed, A. H. *Int. Polym. Proc.* **2013**, *28*, 3.
12. Potschke, P.; Arnaldo, M. H.; Radusch, H. J. *Polimery* **2012**, *57*, 204.
13. Wang, D.; Song, P.; Liu, C.; Wu, W.; Fan, S. *Nanotechnology* **2008**, *19*, 075609.
14. Du, F.; Fischer, J. E.; Winey, K. I. *Phys. Rev. B* **2005**, *72*, 121404.
15. Fangming, D.; Fischer, J. E.; Winey, K. L. *Phys. Rev. B* **2005**, *72*, 121404.
16. Potschke, P.; Brunig, H.; Janke, A.; Fischer, D.; Jehnichen, D. *Polymer* **2005**, *46*, 10355.
17. Letwimolnun, W.; Vergnes, B.; Ausias, G.; Carreau, P. J. *J. Non-Newtonian Fluid Mech.* **2007**, *141*, 167.
18. Ren, J. X.; Krishnamoorti, R. *Macromolecules* **2003**, *36*, 4443.
19. Perrin, F. *J. Phys. Radium Ser. VII* **1934**, *5*, 303.
20. Solomon, M. J.; Almusallam, A. S.; Seefeldt, K. F.; Somwangthanaroj, A.; Varadan, P. *Macromolecules* **2001**, *34*, 1864.
21. Lele, A.; Mackley, M.; Galgali, G.; Ramesh, C. *J. Rheol.* **2002**, *46*, 1091.
22. Nazockdast, E.; Nazockdast, H. *Appl. Rheol.* **2011**, *21*, 25434.
23. Folgar, E.; Tucker, C. L. *J. Reinf. Plast. Comp.* **1984**, *3*, 98.
24. Lipscomb, G. G.; Denn, M. M.; Hur, D.; Boger, D. V. *J. Non-Newtonian Fluid Mech.* **1988**, *26*, 297.
25. Morrison, F. A. Understanding Rheology; Oxford University Press: New York, **2001**.
26. Khalkhal, F.; Carreau, P. J. *J. Non-Newtonian Fluid Mech.* **2012**, *171*, 56.
27. Yang, M.; Wang, P.; Huang, C. Y.; Sherry, M.; Liu, H.; Gogos, C. *Int. J. Pharm.* **2010**, *395*, 53.
28. Croce, F.; Appetecchi, G. B.; Persi, L.; Scrosati, B. *Nature* **1998**, *394*, 456.
29. Song, Y. S. *Rheol. Acta* **2006**, *46*, 231.
30. Nazockdast, E.; Nazockdast, H.; Goharpey, F. *Polym. Eng. Sci.* **2008**, *48*, 1240.
31. Penu, C.; Hu, G. H.; Fernandez, A.; Marchal, P.; Choplin, L. *Polym. Eng. Sci.* **2012**, *52*, 2173.
32. Mun, S. C.; Kim, M.; Prakashan, K.; Jung, H. J.; Son, Y.; Park, O. *Carbon* **2014**, *67*, 64.
33. Pujari, S.; Rahatekar, S. S.; Gilman, J. W.; Koziol, K. K.; Windle, A.; Burghardt, W. E. *J. Chem. Phys.* **2009**, *130*, 214903.
34. Pujari, S.; Dougherty, L.; Mobuchon, C.; Carreau, P. J.; Heuzey, M. C.; Burghardt, W. R. *Rheol. Acta* **2011**, *50*, 3.
35. Cassagnau, Ph. *Polymer* **2008**, *49*, 2183.
36. Bousmina, M.; Eslami, H.; Grmela, M. Society of Plastics Engineers ANTEC Conference; 67th, **2009**, *1*, 495.
37. Kalfus, J.; Jancar, J. *J. Polym. Sci., Polym. Phys.* **2007**, *45*, 1380.
38. Fan, Z.; Advani, S. G. *Polymer* **2005**, *46*, 5232.
39. Advani, S. G.; Tucker, C. L. *J. Rheol.* **1990**, *34*, 367.